Available online at www.sciencedirect.com
ScienceDirect
International Journal of Mass Spectrometry 257 (2006) 16–26
International Journal of Mass Spectrometry
www.elsevier.com/locate/ijms

Simultaneous determination of analyte concentrations, gas-phase basicities, and proton transfer kinetics using gas chromatography/Fourier transform ion cyclotron resonance mass spectrometry (GC/FT-ICR MS)

Jan E. Szulejko, Zhaohui Luo, Touradj Solouki *

Chemistry Department, 5706 Aubert Hall, University of Maine, Orono, ME 04469-5706, United States

Received 1 November 2005; accepted 22 May 2006
Available online 25 July 2006

Abstract

Details on using analyte gas-phase basicity (GB) or proton affinity (PA) as an additional analysis dimension in GC/FT-ICR MS are reported. Ion–molecule reactions of chemical ionization (CI) reagent ions with the GC separated C_1, C_2, and C_3 aromatic neutral (viz., toluene, *m*-xylene, and mesitylene) and ketone (acetone, 3-pentanone, and 4-heptanone) molecules were monitored. A suite of CI reagent ions was generated by self-chemical ionization (SCI) of ethanol in an ICR cell. Multiplexed reactant ion monitoring (MRIM) of the CI reagent ions (R_iH^+) was used for GB bracketing of the neutral analytes eluting from the GC column. The PAs of the conjugate bases (R_i) of the reagent/reactant ions spanned a wide range (~170 to ~200 kcal mol^{-1}). A kinetic model was constructed to relate the degree of reactant ion depletion to analyte concentration and proton transfer reaction efficiency. Our experimental GB estimations, based on the thermokinetic data, were in broad agreement with the GB values reported in the NIST database and primary sources (experimental and ab initio). Experimentally measured MRIM chromatogram profiles and kinetic analysis were used to estimate analyte gas-phase pressures in the ICR cell and losses to the surfaces in the ICR vacuum chamber. The MRIM approach permits GB determinations of multiple analytes in a single GC run and provides an additional dimension to improve analytical resolution in GC/FT-ICR MS.

Keywords: Gas-phase basicity (GB); GC/FT-ICR MS; Multiplexed reactant ion monitoring (MRIM); Proton affinity (PA); Thermokinetic

1. Introduction

In conventional gas chromatography mass spectrometry (GC/MS) experiments, analyte retention time (RT) and mass spectral appearances are used for unknown identification. The retention times and analyte elution order depend on a number of GC experimental variable parameters such as the column type, carrier gas type, temperature and/or pressure programming. For this reason, analyte identifications by GC/MS and the reference library searches rely on mass spectral data only. However, mass spectral library databases may not contain data for a truly unknown analyte [1] and additional analysis dimensions may be needed. To improve analytical resolution and unknown identification, it is desirable to introduce other dimensions of analyses that can provide complementary structural and/or thermochemical information. For example, determination of the proton affinity (PA) or ionization energy (IE) of an analyte, concurrent with its GC/MS analysis and quantification, can provide data in an additional dimension to improve GC/MS analysis.

In this paper, we describe an analytical approach for concurrent identification of analyte gas-phase basicities (and proton affinities) in GC Fourier transform ion cyclotron resonance (GC/FT-ICR) mass spectrometry. Moreover, we show that analyte concentrations in the ICR cell can be estimated by using the thermochemical/kinetic data.

Reviews on the merits of multidimensional analysis approaches in GC [2,3] and GC/MS [4] have been published. In general, EI ionization is considered to be a "hard" ionization technique and EI mass spectra have rich fragment ion information content for unknown identification; conversely, the "softer" CI mass spectra offer molecular weight, functional group [5,6], and proton affinity (PA) information.

Munson and coworkers previously reported on the utility of reactant ion monitoring (RIM) for analyte quantification [7] and

* Corresponding author. Tel.: +1 201 581 1172; fax: +1 207 581 1191.
E-mail address: solouki@maine.edu (T. Solouki).

1387-3806/$ – see front matter © 2006 Elsevier B.V. All rights reserved.
doi:10.1016/j.ijms.2006.05.016

proton affinity bracketing [8]. They used chemical ionization of methane and other reagents to generate the desired reagent ions at 0.5–2 Torr[1] ion source pressures on a sector mass spectrometer. More recently, Tabert et al. [9] reported on the potential of using an array of four miniature CI cylindrical ion traps to acquire multiplexed CI (and EI) mass spectra of a sample to improve analytical resolution. Grützmacher and coworkers used "ion-titration" to resolve a mixture of isomeric analytes using FT-ICR. In the "ion-titration" method, an isomeric reactant ion mixture was generated and the analyte reactions with a suite of reference bases were monitored to determine gas-phase acidities and relative abundance of the isomeric ions [10].

Here, we utilize multiplexed reactant ion monitoring (MRIM) to acquire thermochemical data and analyte concentrations for GC eluting compounds. We use self-chemical ionization (SCI) of ethanol to generate and trap various reactant ions inside the ICR cell. We show that, in a single GC/FT-ICR MS experiment, degrees of CI reactant ion depletions can be monitored to obtain thermochemical data for GC eluting analytes.

2. Experimental

2.1. Instrumentation

All experiments were performed on an in-house designed [11,12] 7-T GC/FT-ICR MS (IonSpec Corp., Forest Lake, CA). The instrument is equipped with an SRI model 8610C GC (SRI Instruments, Las Vegas, NV) and an in-house configured cryofocusing GC/FT-ICR MS interface based on a Jacoby et al. design [13]. A 60 m (0.28 mm i.d., 3 μm crossbonded 100% dimethyl polysiloxane stationary phase coating) MXT-1 capillary column (Restek Corp., Bellefonte, PA) was used for all GC experiments. The vacuum chamber surrounding the ICR cell was maintained at ∼87 ± 5 °C by a set of DC heating elements [14].

A brief description of the ICR cell, EI filament, and vacuum chamber is provided below to give an idea of their relative locations and dimensions. The EI filament ribbon was supported and isolated by Macor blocks and mounted on one of the two trapping plates of a ∼15 cm long × 6 cm diameter segmented cylindrical ICR cell. The ion cloud was trapped ∼7.5 cm away from the EI filament and in the center of the ICR cell. The ICR cell was located at the blind end of a ∼70 cm long × 10 cm diameter internally polished vacuum chamber. This vacuum chamber was pumped by two 220 L s^{-1} turbomolecular drag pumps through a separate vacuum housing. A third 220 L s^{-1} turbomolecular pump was connected to an external ion source region (IonSpec Corp., Forest Lake, CA). In the experiments discussed here, all ions were generated in the internal ionization modes and the external ion source was not used. Compared to the relative pumping speeds of the turbo pumps, conductance or gas flow between the external ion source region and the main chamber was negligible. The ICR cell assembly was supported at the end of a quadrupole ion-guide assembly. The EI filament and the GC transfer line were positioned centrally and on the opposing trapping plates (i.e., "filament" and "quad" trapping plates, respectively). The end of the ∼1 m long GC transfer line (from the pulsed valve interface) was positioned on the *z*-axis at the end of the quadrupole rod assembly, ∼2 mm from the "quad" trapping plate. Numerous 3 mm diameter holes were drilled in the trapping plates (both on the EI filament and quadrupole side) to improve gas flow out of the ICR cell.

2.2. GC programming

The GC programming used in all experiments was as follows: initialize at 60 °C for 2 min, ramp at 3 °C/min to 180 °C and isothermal at 180 °C for experiments exceeding 42 min. The carrier gas (He) head pressure was 15 psi.

2.3. Chemicals and sample preparation

Mesitylene (98%), *m*-xylene (99+%), and ketones were purchased from Sigma–Aldrich Chemical Company, Inc. (Milwaukee, WI). Ethanol (ACS/UPS grade 200 proof) and toluene (ACS certified purity) were purchased from Pharmco (Brookfield, CT) and Fisher Scientific, respectively; all chemicals were used as received. Two head-space sample mixtures were prepared. First mixture contained toluene, *m*-xylene, and mesitylene and the second mixture contained acetone, 3-pentanone, and 4-heptanone. These mixtures were prepared by injecting ∼0.5 μL of each liquid into septum sealed 40-mL vials containing N_2 at 1 atm. The calculated 1.7 Torr partial pressure of mesitylene (the least volatile analyte) for a 0.5 μL liquid sample in the 40-mL vial is below its saturated vapor pressure (SVP) of 2.5 Torr at 25 °C [15]. For all of the GC/FT-ICR experiments reported here, we used 50 μL head-space samples withdrawn from the 40-mL mixture vials.

2.4. Introduction of the ethanol chemical ionization reagent

A 250 mL reservoir connected to a pulsed valve contained ethanol at a pressure of ∼1 Torr. Conventional freeze–pump–thaw cycles were used for ethanol degassing prior to admittance to the evacuated 250 mL reservoir. Gaseous ethanol from the reservoir was used to generate the CI reagent/reactant ions. The ethanol reagent was pulsed into the main vacuum housing through a port located ∼30 cm above the two turbomolecular drag pumps and ∼90 cm from the center of the ICR cell (IonSpec Corp., Forest Lake, CA).

2.5. Pressure measurements

The pressure transients of the ethanol SCI reagent and GC effluent pulsed into the ICR cell were recorded to estimate instrumental pump down characteristics. The analog output from the Granville-Phillips (series 350) ionization gauge controller (Boulder, CO) was recorded using a LeCroy 9300C Series digital oscilloscope (Chestnut Ridge, NY). The ion gauge tube was located ∼90 cm from the ICR cell and ∼30 cm above the turbomolecular pump closest to the ICR cell (IonSpec Corp., Forest Lake, CA).

[1] 1 Torr = 133 bar.

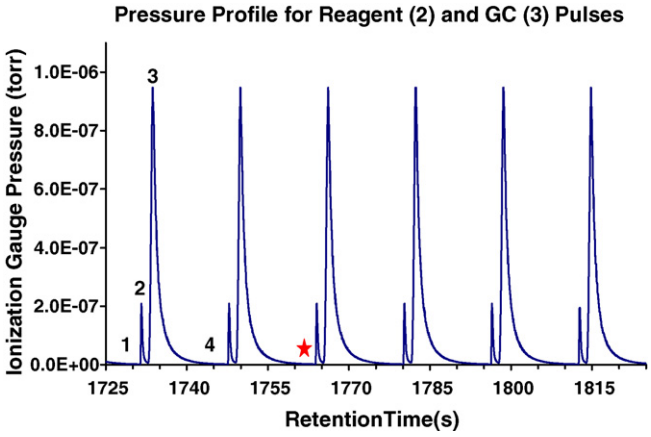

Fig. 1. The ICR vacuum chamber pressure profiles during the CI GC/FT-ICR MS data acquisition. The analog output from the Granville-Phillips (series 350) ionization gauge controller (Boulder, CO) was recorded to construct the ICR pressure profiles. After removing all of the trapped ions (ion quench labeled as point 1), the ethanol reagent gas was introduced into the ICR cell via a pulsed-valve during 0–8 ms interval (labeled as point 2). Ethanol was ionized at 70 eV electron energy and reactant ions (i.e., ions at m/z 31, 43, 45, 47, 75, and 93) were formed. The GC eluent was pulsed into the ICR cell (labeled as point 3) and GC separated analytes (e.g., toluene, *m*-xylene, and mesitylene) were allowed to react with the reactant ions. After allowing ~12 s for the ion–molecule reactions, mass spectra were recorded (labeled as point 4). The retention time labeled with the star corresponds to the detection of *m*-xylene (see Fig. 3).

The voltage output (V_o) of the ionization gauge controller is a linear function of the logarithm of the pressure. This voltage output (V_o) was converted to vacuum chamber pressure (P, Torr) using $V_o = \log(P) + C$ type relationship. In order to determine the value of C, we used two measurements at the steady pressures of 4.8×10^{-6} Torr (for high pressure) and 2.8×10^{-10} Torr (for base pressure). Our experimentally measured value of -10.9 for C was in close agreement with the value of -11 provided in the Granville-Phillips instruction manual (Catalog No. 350010). To generate the pressure plots shown in Fig. 1 (GC retention time {RT} versus ionization gauge pressure readout), the digitized ASCII data from the oscilloscope (sampling rate = 50 Hz) were transferred to a PC and plotted using Origin 7.0 (Northampton, MA).

3. Kinetic schemes

3.1. General comments

A bimolecular ion–molecule kinetic scheme similar to that reported in references [16,17] was used to model the single ion chromatograms (SICs) of CI reagent ions. Using the MRIM approach, analyte concentrations and proton transfer reaction efficiencies could be determined simultaneously. Gas-phase basicities were determined based on the thermokinetic method of Bouchoux et al. [18]. In an earlier GC/MS work of Tran and Munson [8], the occurrence or non-occurrence of a proton transfer reaction was used for PA (or gas-phase basicity) bracketing. Here, we use a thermokinetic method to determine analyte gas-phase basicities with improved accuracy (± 1 kcal mol^{-1})[2] [18].

[2] 1 cal = 4.184 J.

In principle, the use of thermokinetic method [18] (instead of using the occurrence or non-occurrence of proton transfer reactions) should yield more accurate GB results.

3.2. Kinetic modeling

Only a single GC/FT-ICR MS experiment was required to calculate gas-phase basicities and analyte concentrations for multiple analytes. Therefore, the need to perform auxiliary experiments on each analyte to measure its gas-phase basicity and/or concentration was avoided.

We used a bimolecular ion–molecule reaction (Eq. (1)) and a pseudo second order kinetic (Eq. (2)) scheme to model the attenuation of a reactant ion's abundance in the presence of an analyte in the ICR cell. The observed attenuation of the reactant ion's abundance, as measured from its selected ion chromatogram (SIC), was used to estimate the gas-phase analyte concentrations in the ICR cell and basicities. In addition, auxiliary equations were used to extract further information content from the SIC, such as, reaction rate efficiencies for proton transfer and hence the GB of an analyte. The procedure used to extract data from SIC profiles is described below in more detail.

Consider the proton transfer reaction between the ith CI reagent/reactant ion (R_iH^+) and the jth analyte (A_j) occurring in the ICR cell (Eq. (1)) with a rate constant of k_{ij}:

$$R_iH^+ + A_j \rightarrow A_{ij}H^+ + R_i \quad (1)$$

$$d[R_iH^+]/dt = -k_{ij}[R_iH^+][A_j] \quad (2)$$

The disappearance of $[R_iH^+]$ is governed by Eq. (2), where $[A_j]$ is the concentration of jth analyte in the ICR cell and $[R_iH^+]$ is the concentration of a given CI reagent ion (A_j) at a reaction time, t. In Eq. (1), $A_{ij}H^+$ denotes the protonated product from the reaction of the ith reagent with the jth analyte.

From the pressure measurements (see Section 4.1), it was observed that after the GC effluent introduction, the ion gauge pressure reading decayed at a rate of 1.5 s per decade (or a time constant, $\tau_{He} \sim 0.65$ s) for helium. The pressure decay time constant (τ_j) for an analyte is proportional to $m_j^{0.5}$ where m_j is the analyte molecular weight. The τ_j for a given analyte is estimated using Eq. (3) (from Graham's law). After the GC effluent introduction event, the analyte concentration at reaction time, t, is given by Eq. (4):

$$\tau_j = (\tau_{He})(m_j/m_{He})^{0.5} \quad (3)$$

$$[A_j] = [A_j]_0 \exp(-t/\tau_j) \quad (4)$$

where $[A_j]_0$ is the maximum analyte concentration in the ICR cell environs after the GC effluent introduction event.

Substituting $[A_j]$ from Eq. (4) into Eq. (2) and integrating yields:

$$\ln([R_iH^+]) = k_{ij}[A_j]_0\tau_j \exp(-t/\tau_j) + \text{constant} \quad (5)$$

At $t = 0$, $[R_iH^+] = [R_iH^+]_0$, where $[R_iH^+]_0$ is the abundance of R_iH^+ reagent ion (at the SIC "baseline") when no analyte is present in the ICR cell (e.g., at a retention time of 1500 s in

Figs. 3 and 5). Hence

$$\ln([R_iH^+]/[R_iH^+]_0) = -k_{ij}[A_j]_0\tau_j[1 - \exp(-t/\tau_j)] \equiv \ln(\varepsilon_{ij}) \quad (6)$$

For a given reagent ion (i) and an analyte (j) couple, the ratio ($[R_iH^+]/[R_iH^+]_0$) in Eq. (6), will be denoted as ε_{ij} in the text below. The reaction delay time (t) (in Eq. (6)) is referenced to the analyte introduction (from the GC to the ICR cell).

Using the experimental τ_{He} of ~0.65 s for helium in Eq. (3), an estimated gas-phase pressure decay time constant (τ_{mx}) for m-xylene (mol. wt. = 106) was estimated to be ~3.35 s ($0.65\{106/4\}^{0.5}$ s). The CI reaction time in some experiments was 9 s which is $\sim 2.7\tau_{mx}$. Therefore, at the detection event, the m-xylene concentration had decayed to ~0.07 of $[A_j]_0$ which may be sufficient to produce "tailing" on the SIC GC peak. From Eq. (6), the analyte concentration, $[A_j]_0$ (molecules cm^3), near the GC effluent introduction event can be calculated assuming a Langevin rate constant (k_{Lg}) of 2×10^{-9} molecule^{-1} cm^3 s^{-1} for an exothermic proton transfer reaction. To reduce experimental errors we used a practical range of 0.05 to 0.95 for ε_{ij} values (at the extreme values, small errors in ε_{ij} yields large errors in η_{ij} {see Eq. (9)}); as the analyte concentration approaches zero (i.e., at the lower concentrations), the $[A_{ij}H^+]/[R_iH^+]_0$ ratio becomes linear in $[A_j]$.

The CI dynamic range on our instrument is approximately three orders of magnitude and non-linear except at low analyte concentrations. This small and non-linear dynamic range precludes the determination of proton affinities for analytes at either very low or high concentrations (or pressures) in the ICR cell. The upper and lower experimental pressure limits (Torr) in the ICR cell can be estimated from Eq. (6) using (ε_{ij}) values of 0.95 (lowest practical reactant ion depletion) and 0.05 (highest practical reactant ion depletion); using $k_{ij} = 2 \times 10^{-9}$ molecule^{-1} cm^3 s^{-1}, $\tau_j = 3.3$ s, $T = 360$ K, and CI reaction time of $t = 9$ s in Eq. (6), yields an estimated practical analyte pressure (i.e., $[A_j]_0$) range of $\sim 3 \times 10^{-10}$ to $\sim 2 \times 10^{-8}$ Torr. For samples sizes that yield ICR cell analyte pressures outside of this operational range, the amount of analyte injected onto the GC column can be adjusted appropriately. Alternatively, one can use CI reagent ions that are not completely depleted (acceptable range for the ion depletion is 5–95%) and extract relative reaction efficiencies and GB using the thermokinetic method [18].

3.3. Gas-phase basicities and proton affinities

The rate constant (k_{ij}) for an endoergic proton transfer reaction will be smaller than k_{Lg} and therefore ε_{ij} will be larger compared to an exoergic proton transfer reaction. The proton transfer rate constant (k_{ij}) for a given reagent ion (i) and an analyte (j) is obtained from Eq. (6) upon rearrangement (Eq. (7)). For an exoergic proton transfer reaction ($\Delta G_{ij} < -3$ kcal mol^{-1}), k_{ij} is assumed to be near Langevin collision rate constant (k_{Lg}), i.e., $k_{ij} = k_{Lg}$:

$$k_{ij} = -\ln(\varepsilon_{ij})/\{[A_j]_0\tau_j[1 - \exp(-t/\tau_j)]\} \quad (7)$$

The reaction efficiency (η_{ij}) for a proton transfer reaction is given by Eq. (8):

$$\eta_{ij} = k_{ij}/k_{Lg} \quad (8)$$

where k_{Lg} is the rate constant for an exothermic proton transfer reaction (assumed to be close to the Langevin rate constant of $\sim 2.0 \times 10^{-9}$ molecule^{-1} cm^3 s^{-1}).

The η_{ij} values were calculated using the reactant ion SIC minima values corresponding to the analyte retention times where the CI reagent ion depletions were at maximum. In our analysis, an exact value for k_{Lg} was not required to calculate η_{ij}. The ratio (η_{ij}) was referenced with respect to fast proton transfer reactions between an analyte and reactant ion(s) of lowest conjugate proton affinity/affinities. Hence

$$\eta_{ij} = \ln(\varepsilon_{ij})/\ln(\varepsilon_{Lg}) \quad (9)$$

where the subscripts ij and Lg denote endoergic and exoergic (near Langevin collision rate) proton transfer reactions to a given analyte, respectively. The value for ε_{Lg} is calculated using the RIM data obtained on the reagent ion(s) of low or lowest conjugate base proton affinity for which k_{Lg} was assumed.

It should be noted that neither the analyte concentration in the ICR cell nor the actual proton transfer rate constants need to be known explicitly in order to estimate the GB of an analyte. Our approach is similar to that used by Hatch and Munson [16] and Lin et al. [17] to obtain unknown rate constants referenced to a reaction of a known rate constant, i.e., see Eq. (15) in Ref. [16].

Based on the thermokinetic method [18], the gas-phase basicity of an analyte, $GB(A_j)$, can be determined by using Eq. (10):

$$GB(A_j) = GB(R_i) + RT\ln(1/\eta_{ij} - 1) - \Delta G_a \quad (10)$$

$$\Delta G_{ij} = GB(R_i) - GB(A_j) = RT\ln(1/\eta_{ij} - 1) - \Delta G_a \quad (11)$$

where T is the effective temperature of the ions inside the ICR cell (ICR vacuum chamber temperature ~87 °C), $GB(R_i)$ the gas-phase basicity of the conjugate base of the reactant ion, ΔG_a an apparent activation barrier (normally small), and R is the gas constant (1.987 cal mol^{-1} K^{-1}). In Eq. (11), ΔG_{ij} is the ergicity for proton transfer from R_iH^+ to A_j. For our purposes, we have set $\Delta G_a = 0$, and $T = 360$ K. See the discussion on Fig. 6 in Section 4.5.2 for supporting commentary on assigning $\Delta G_a = 0.0$.

Setting $T = 360$ K is a reasonable assumption under our ICR conditions where the estimated maximum He pressure in the ICR cell was $\sim 7 \times 10^{-4}$ Torr ensuring a high degree of thermalization for both reactants and products (see Section 4.4 for further details). It should be noted that the thermokinetic method (based on reaction efficiencies) measures the free energy change (i.e., ΔG_{ij}, Eq. (11)) and not the enthalpy (i.e., ΔH_{ij}) of a proton transfer reaction [18,19]. To estimate the ΔH_{ij} value, a reasonable estimate of the entropy contribution (ΔS_{ij}) to ΔG_{ij} at the given temperature must be available (see Section 4).

To obtain the GB for an analyte, ε_{ij} should be in the range of 0.1 to 0.9 and η_{ij} less than 0.7. For $\eta_{ij} > 0.7$ or < 0.05, small variations in η_{ij} will cause large changes in $GB(A_j)$ compared to when $0.05 < \eta_{ij} < 0.7$; for example, as seen in Fig. 6, a small change in η_{ij} on either side of the transition zone (i.e., transition

zone defined as $0.05 < \eta_{ij} < 0.7$) will result in large changes in ΔG_{ij}. Therefore, for $\eta_{ij} < 0.05$ and $\eta_{ij} > 0.7$, the GB estimation, using Eq. (10), should be evaluated with caution.

4. Results and discussion

4.1. Pressure measurements

In Fig. 1, pressure transients for six mass spectral data acquisitions (RT = 1725–1825 s) are shown; the various events have been labeled for the first mass spectral data point (labels 1–4 for RT ~ 1731–1747 s) in the set. These events are: (1) ion ejection/removal from the ICR cell (where pressure was at its lowest), (2) introduction of the ethanol CI reagent, (3) GC eluent introduction, and (4) mass spectral detection.

Typically, reagent (or reactant) ions were generated between the events 2 and 3. For example, electron impact ionization of the reagent gas occurred for 300 ms (t = 0–0.3 s after the pulsed introduction of the CI reagent, here $t = 0$ is defined as the time when CI pulsed valve opens) and subsequently SCI was allowed to occur up to the GC eluent's pulsed introduction (i.e., from 0 to 2.2 s). The GC eluent was pulsed into the ICR cell at $t \sim 2.2$–3.0 s. Mass spectra were recorded 15 s after the CI reagent introduction (label 4 in Fig. 1, where background pressure was sufficiently low to excite and detect ions). For example, the star at the retention time ~1763 s corresponds to the elution and chemical ionization of *m*-xylene (e.g., corresponding to a GC ion chromatogram peak for *m/z* 107 in Fig. 3); the resulting CI mass spectrum for *m*-xylene is shown in Fig. 4b. The GC eluent was pulsed into the ICR cell (labeled as point 3) and GC separated analytes (e.g., toluene, *m*-xylene, and mesitylene) were allowed to react with the reactant ions. After allowing ~12 s for the ion–molecule reactions, mass spectra were recorded (labeled as point 4). There was a 1 s delay between mass spectral points.

The maximum ethanol pressure of $\sim 2 \times 10^{-7}$ Torr was reached ~200 ms after the 8 ms duration pulsed valve event. Similarly, the maximum GC eluent pressure of $\sim 1 \times 10^{-6}$ Torr was measured ~200 ms after the GC/FT-ICR interface pulsed valve was opened. The GC eluent pressure decayed at an initial rate of ~1.5 s per decade from its peak value of $\sim 1 \times 10^{-6}$ to $\sim 2 \times 10^{-8}$ Torr. Subsequently, the pressure decayed more slowly to reach a pressure of $\sim 2 \times 10^{-9}$ Torr at the excite/detect event (label 4 in Fig. 2) which is higher than the base pressure (i.e., $\sim 2.8 \times 10^{-10}$ Torr) of the instrument. The slower pressure decay rate at lower pressures and the non attainment of the instrument base pressure 12 s after the GC eluent introduction was mostly due to analyte and residual helium desorption off various surfaces. As shown in Fig. 1, the pressure transient profiles were reproducible.

The experimental temperature of the vacuum chamber surrounding the ICR cell (87 ± 5 °C) was significantly lower than the higher detector temperatures (≥200 °C) used in conventional GC/MS; higher temperatures are used to reduce/eliminate absorption on "cold spots". Heating the ICR cell environs beyond ~90 °C was impractical due to out-gassing of the heat sensitive ICR cell components. The pressure decay rate is also reduced by the presence of ICR cell support components, such as the quadrupole assembly, inside the vacuum chamber.

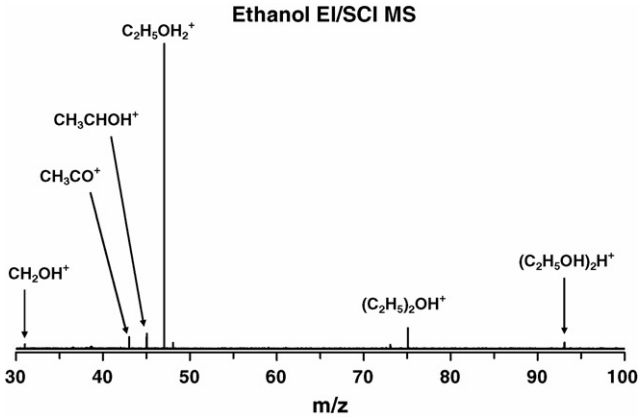

Fig. 2. EI/SCI FT-ICR mass spectrum of ethanol at the GC retention time of 1550 s. The reactant ions were either EI (at *m/z* 31, 43, and 45) or SCI (at *m/z* 47, 75, and 93) product ions from ethanol. At the RT ~ 1550 s, no GC eluting analytes (apart for the He carrier gas) were present in the ICR cell to react with the reactant ions and hence ions at *m/z* 31, 43, 45, 47, 75, and 93 were not attenuated.

4.2. Reactant ion and analyte literature gas-phase thermochemical data

The gas-phase basicity of a base B, GB(B), is related to its PA(B) and protonation half-reaction entropy change $\{\Delta_p S^\circ(B)\}$:

$$\mathrm{GB(B)} = \mathrm{PA(B)} - T\{S^\circ_{H^+} + \Delta_p S^\circ(B)\} \quad (12)$$

where $S^\circ_{H^+}$ is the translational entropy of H^+ (26.9 cal mol^{-1} K^{-1} at 360 K), and $\Delta_p S^\circ(B) = S^\circ(BH^+) - S^\circ(B)$ is the protonation half-reaction entropy defined as the entropy difference between the protonated base, $S^\circ(BH^+)$, and neutral base $S^\circ(B)$. The NIST $\Delta_p S^\circ$ values in Table 1 were calculated using Eq. (12) and the NIST PA and GB_{298} data. It should be noted that both PA and $\Delta_p S^\circ$ vary slightly with temperature and this effect will not be considered here to simplify the discussion. Student's *t*-tests on the PA and GB_{298} data (in Table 1) showed that the primary versus NIST data at the 90% confidence level are statistically indistinguishable.

Three primary literature sources on $\Delta_p S^\circ$ data were used to calculate GB at T = 360 K, viz., from high pressure mass spectrometry (HPMS) data (500 K $\Delta_p S^\circ$) [20,21] and high level quantum mechanics (linearly interpolated 500 K $\Delta_p S^\circ$ values) [22].

Table 1 contains the relevant thermochemical data for all analytes and reagent ions used in this study. The first column in Table 1 contains the chemical names of the neutral analytes (A) and neutral conjugate bases (R) of the reagent ions. Entries in columns 2 and 3 correspond to 298 K gas-phase basicities from the primary sources in the literature and NIST. Proton affinities from the primary sources in the literature and NIST are listed in columns 4 and 5. The half-reaction entropy changes for proton transfer ($\Delta_p S^\circ$) from the primary sources in the literature (500 K) and NIST (298 K) are listed in columns 6 and 7, respectively. Columns 8 and 9 contain the calculated gas-phase

Table 1
Literature gas-phase basicity, proton affinity, and half-reaction protonation entropy thermochemical data for all bases used or studied in present work

Base (analyte (A) or reagent (R))	GB_{298} (kcal mol^{-1})		PA (kcal mol^{-1})		Δ_pS° (cal mol^{-1} K^{-1})		GB_{360} (kcal mol^{-1})	
	Primary Ref.	NIST	Primary Ref.	NIST	Primary Ref.	NIST	Primary Ref.	NIST
Formaldehyde (R)	163.4[a]	163.3	170.1[a]	170.4	3.5[a]	2.2	161.7	161.5
Acetaldehyde (R)	176.8[a]	176.0	184.1[a]	183.7	1.5[a]	0.2	175.0	174.1
Ethanol (R)	ND	178.0	ND	185.6	ND	0.5	ND	176.1
Toluene (A)	180.8[b]	180.8	187.7[b]	187.4	3.0[b]	3.9	179.1	179.1
m-Xylene (A)	186.6[c]	186.9	192.3[c]	194.0	7.0[c]	2.2	185.1	185.1
Acetone (A)	187.1[b]	187.9	194.0[b]	194.1	3.0[b]	5.2	185.4	186.3
Ketene (R)	189.6[a]	189.7	197.0[a]	197.3	1.0[a]	0.5	187.7	187.8
Ether (R)	191.4[b]	191.0	198.1[b]	198.0	3.5[b]	2.5	189.7	189.2
3-Pentanone (A)	192.3[b]	193.3	199.3[b]	199.9	2.5[b]	3.9	190.5	191.6
Mesitylene (A)	192.7[c]	193.0	198.5[c]	200.0	6.5[c]	2.5	191.2	191.2
4-Heptanone (A)	195.0[d]	194.7	201.9[d]	202.0	3.0[d]	1.5	193.3	192.9

ND: no data available from Refs. [20–22]; used NIST PA and GB_{298} data to calculate NIST Δ_pS° ($\Delta_pS^\circ = 26.0 + (GB_{298} - PA)/0.298$) and hence $GB_{360} = PA - 0.360(26.9 - \Delta_pS^\circ)$. NIST: NIST online (http://nist.gov) chemistry webbook.
[a] Ref. [22].
[b] Ref. [20].
[c] Ref. [21].
[d] J.E. Szulejko, Unpublished Proton Affinity Database Based on 1984–1998 HPMS Data from Laboratory of Prof. T.B. McMahon University of Waterloo, Ont., Canada (copies are available upon request from the authors).

basicities (GB_{360}) based on the PA and Δ_pS° values from the primary sources in the literature and NIST.

4.3. Self-chemical ionization of ethanol reagent and proton transfer to analytes

In the absence of any analytes eluting from GC, only He carrier gas atoms were present in the ICR cell and hence the acquired mass spectra contained the "none consumed" or "non attenuated" CI reactant ions. For example, the mass spectrum in Fig. 2 corresponds to RT ~ 1550 s in Fig. 3, and the "none consumed" ions present in the mass spectrum include *m/z* 31, 43, 45, 47, 75, and 93; these ions are all from EI and SCI reactions

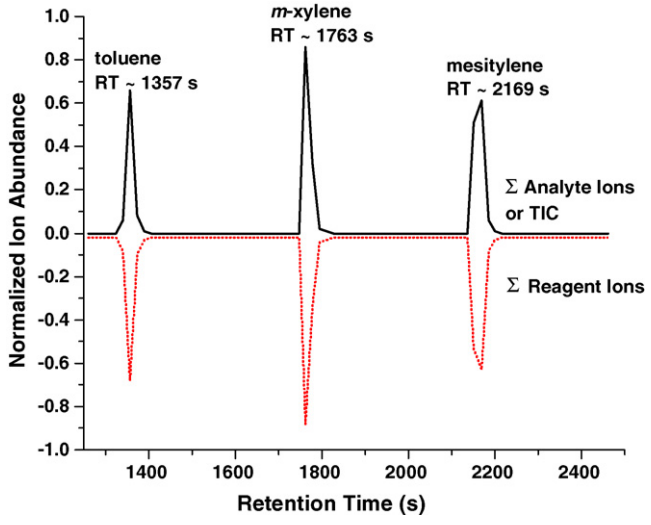

Fig. 3. The chromatograms for sum (Σ) of the protonated analyte ions (viz., *m/z* 93, 107, and 121—solid line, positive going curve showing product generation), and sum (Σ) of reactant ions (viz., 31, 43, 45, 47s, and 75—dotted line, negative going curve showing reactant depletion) for a representative GC/FT-ICR MS trial in the CI mode.

of ethanol and their chemical identities are indicated in Fig. 2; thermochemical data for reagent ions are provided in Table 1. When an analyte elutes from the GC transfer line and enters into the ICR cell, CI product ions can be formed. For instance, mass spectra shown in Fig. 4a–c correspond to retention times of toluene (RT ~ 1357 s), *m*-xylene (RT = 1763 s), and mesitylene (RT = 2169 s). The degree of reagent ion depletion and product ion formation depends on the analyte pressure and ergicity of the proton transfer reaction.

In the mass spectrum shown in Fig. 2, protonated ethanol (*m/z* 47) is the major peak (100% relative abundance) observed in the SCI mass spectrum. The other peaks corresponds to ions at *m/z* 31 (protonated formaldehyde, an ethanol EI fragment ion), *m/z* 43 (largely protonated ketene, an ethanol EI fragment ion) [23], *m/z* 45 (protonated acetaldehyde, an ethanol EI fragment ion) [24] and *m/z* 75 (protonated ether, an ion–molecule reaction product of protonated ethanol with neutral ethanol) [25], and *m/z* 93 (the proton bound dimer of ethanol, an association reaction product of protonated ethanol with ethanol) [25]. The PA of the conjugate base of the reagent ion at *m/z* 93 (proton bound dimer of ethanol, $PA \equiv -\Delta H \equiv 217.0$ kcal mol^{-1} [26] for $EtOH + EtOH + H^+ \rightarrow \{EtOH\}_2H^+$) is higher than any of the analytes included in our study and therefore *m/z* 93 was not included in the MRIM kinetic analyses.

4.4. Ion cooling considerations

On the μs timescale, most of the *m/z* 43 generated from 70 eV EI on ethanol is ketene protonated on the terminal C site (viz., $[CH_3CO]^+$). The minor component is ketene protonated on the O site (viz., $[CH_2COH]^+$). This higher energy species, $[CH_2COH]^+$, may collapse quantitatively to $[CH_3CO]^+$ via a proton transport catalysis mechanism [27] induced by collisions mainly with helium eluting off the GC and to a lesser extent, ethanol.

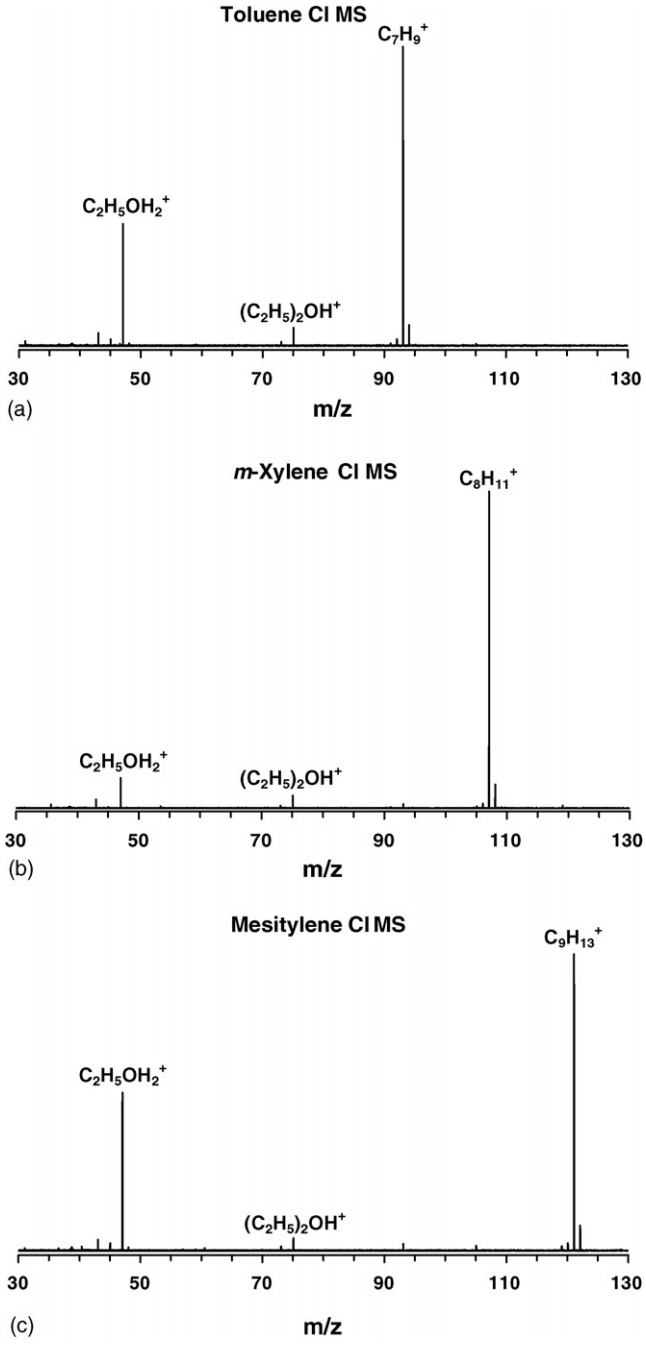

Fig. 4. The CI/FT-ICR mass spectra for (a) toluene (RT ~ 1357 s in Fig. 3), (b) *m*-xylene (RT ~ 1763 s in Fig. 3), and (c) mesitylene (RT ~ 2169 s in Fig. 3).

The pumping speed for He ($S_c \sim 3\,L\,s^{-1}$) in the environs of the ICR cell can be estimated using $S_c = V_c/\tau_{He}$ (from $V_c dP_c/dt = P_c S_c$) where V_c (~2 L) is the approximate volume of the vacuum chamber surrounding the ICR cell, τ_{He} (~0.65 s calculated from the pressure decay observed in Fig. 1) is the helium pump down time constant, and P_c is the ICR cell pressure $\{P_c = P_{cm}\exp(-t/\tau_{He})$ where P_{cm} is the maximum He pressure$\}$. At the molecular flow region and with no physical obstruction present, the conductance for our vacuum chamber $\{\sim 70$ cm long (L) and ~10 cm in diameter (D)$\}$ (Ion-Spec Corp., Lake Forest, CA) would be $\sim 170\,L\,s^{-1}$ ($12D^3/L$) [28]. The maximum He pressure in the ICR cell (P_{cm}) is estimated to be 7×10^{-4} Torr using the data shown in Fig. 1. This pressure was estimated from a mass flow balance relationship $\{P_i S_t = (P_{cm}/C)\cdot S_c\}$ using the following data: the peak ion pressure gauge reading ($P_i = 1 \times 10^{-6}$ Torr, Fig. 1), the total pumping speed ($S_t \sim 400\,L\,s^{-1}$) of the two turbomolecular drag pumps located ~1 m from the ICR cell, an ion gauge correction factor for He ($C = 5$) [29] and the estimated He pumping speed, $S_c \sim 3\,L\,s^{-1}$, near the ICR cell.

The reagent ions (and product ions) were thermalized by the initially high He pressure of $\sim 7 \times 10^{-4}$ Torr present in the ICR cell soon after the GC effluent introduction event. Assuming a calculated Langevin collision rate constant of $k_c = 7 \times 10^{-10}$ molecule^{-1} cm^3 s^{-1} (e.g., $\alpha_{He} = 0.205 \times 10^{-24}$ cm^3) [15] for He with protonated ethanol, the number of reactant ion/helium collisions $\{c = k_c[He]_0\tau_{He}[1 - \exp(-t/\tau_{He})]\}$ for the first second of the He pressure decay was estimated to be 7×10^3. A value of $[He]_0 = \sim 1.9 \times 10^{13}$ atom cm^{-3} was used for the maximum He concentration and $\tau_{He} = 0.65$ s was the He pump down time constant. Even though He is a poor collisional thermalizing agent ($\eta_{He} \sim 0.01$ efficiency compared to near unit efficiency for polyatomics [30]), both the reactant ions and product ions should be thermalized by the ~70 effective collisions (i.e., $c\eta_{He}$). Therefore, in principle, obtaining meaningful thermokinetic data on GC eluting analytes is a realistic goal.

4.5. Multiplexed reactant ion monitoring (MRIM)

4.5.1. MRIM chromatograms

Representative summed MRIM (dotted line, negative going curve denoted as Σ reagent ions in Fig. 3) and summed protonated analyte (solid line, positive going curve denoted as Σ analyte ions or TIC) chromatograms are shown in Fig. 3. The top (solid line) and bottom (dotted line) plots in Fig. 3, show sum of the protonated analyte ion chromatograms (viz., *m/z* 93, 107, and 121) and sum of the reactant ion chromatograms (viz., 31, 43, 45, 47, and 75), respectively. Plots shown in Fig. 3 were normalized with respect to all ions considered (i.e., *m/z* 31, 43, 45, 47, 75, 93, 107, and 121). The chromatogram peaks in Fig. 3 for *m/z* 93, 107, and 121 contained only two or three mass spectra. A long duty cycle of ~15 s was used to reduce the ICR cell pressure during the detection of time domain transient signals (vis-à-vis, pressure decay rates of >1.5 s per decade for He).

When the eluting analytes exit the GC/MS interface and enter into the ICR cell (i.e., during their respective GC retention times of RT ~ 1357 s for toluene, RT ~ 1763 s for *m*-xylene, and RT ~ 2169 s for mesitylene), the total reagent ion abundance (bottom dotted line) is attenuated; this reagent ion signal attenuation is due to proton transfer from the reactant CI reagent ions to the GC eluting analytes. The *y*-scale in Fig. 3 represents the normalized ion abundance; 0 and 1.0 range represents the "no analyte signal" and "maximum analyte signal" (solid line, top plot in Fig. 3), respectively. Conversely, in Fig. 3, 0 to −1.0 range represents "no ion loss" and "total attenuation" of the reagent ion signals (dotted line, bottom plot in Fig. 3). The bottom plot has been shifted (i.e., 2% below zero) for clarity and pictorial

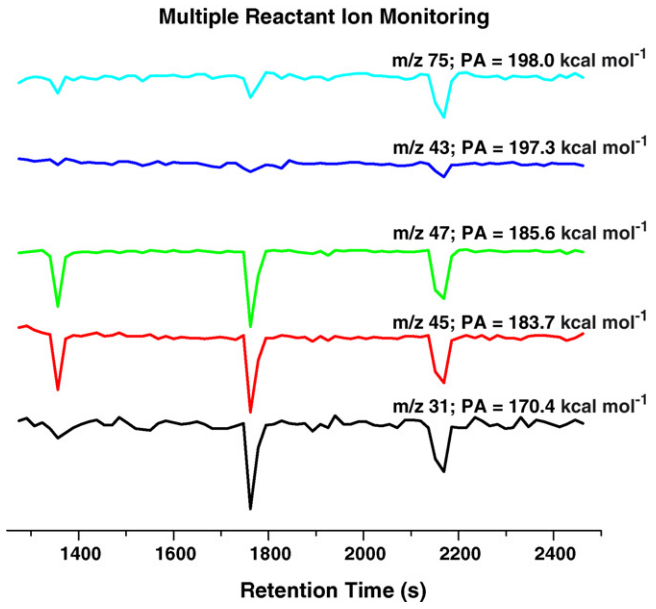

Fig. 5. The reactant ion monitoring plots for *m/z* 31 (conjugate base PA = 170.4 kcal mol^{-1}), *m/z* 45 (conjugate base PA = 183.7 kcal mol^{-1}), *m/z* 47 (conjugate base PA = 185.6 kcal mol^{-1}), *m/z* 43 (conjugate base PA = 197.0 kcal mol^{-1}), and *m/z* 75 (conjugate base PA = 198.0 kcal mol^{-1}).

representation of the data. The two plots in Fig. 3 are mirror images of each other. For example, during the GC elution of all three analytes, the reactant ion concentrations inside the ICR cell are attenuated.

The individual reactant ion chromatograms are shown in Fig. 5 and discussed below. The major reactant ion at *m/z* 47 (protonated ethanol) was still present as a significant peak in all CI mass spectra shown in Fig. 4. Since the *m/z* 47 abundance is not low, this implies that the analyte concentrations in the ICR cell were relatively low in spite of the large analyte injection on the GC. See also the discussion below on analyte losses to surfaces.

A 50 μL sample of head-space from a septum sealed 40-mL vial containing a mixture of toluene, *m*-xylene and mesitylene (0.5 μL each of the liquid analyte in the vial) was injected on the GC. The CI mode GC/FT-ICR mass spectra for toluene, *m*-xylene, and mesitylene are shown in Fig. 4. The major peaks in all mass spectra (Fig. 4a–c) are labeled; the most abundant peak for all three analytes was the protonated pseudo-molecular ion.

The MRIM chromatograms for reactant ions at *m/z* 31, 43, 45, 47, and 75 are shown in Fig. 5 as individually normalized abundance plots. These single ion chromatograms are stacked according to the NIST PA values of their corresponding conjugate bases (in a descending order from top to bottom). In this set of five reactant ions, conjugated bases of the *m/z* 75 and 31 have the highest (PA = 198.0 kcal mol^{-1}) and lowest (PA = 170.4 kcal mol^{-1}) proton affinities. The *y*-axis scale (0–1) for all stacked single ion chromatograms are identical and their separation is 1.05 arbitrary units (*y*-axis scale for each plot is not shown here).

The chromatograms of *m/z* 31, 45, and 47 all have similar depletions for a given analyte as would be expected for reactant ions having much lower conjugate base gas-phase basicities than the analytes. On the other hand, the reactant ions at *m/z* 43 and 75 exhibited less depletion in accord with the proton transfer ergicity being either positive (∼2 kcal mol^{-1}) or marginally negative (∼−1 kcal mol^{-1}). It should be noted that the *m/z* 31 relative abundance is very low (e.g., see Fig. 2) and hence statistical noise becomes significant as noted for the much smaller reactant ion depletion observed for toluene compared to either *m/z* 45 or 47 reactant ions.

4.5.2. Thermokinetic plots of CH_3CO^+ or $(C_2H_5)_2OH^+$ reactant ions with analytes

Due to the small number of reactant ions (R_iH^+) used in this study and their irregular GB(R_i) increments, it was not feasible to plot the proton transfer reaction efficiencies for a given analyte versus the GB(R_i) for the suite of reactant ions. Oth-

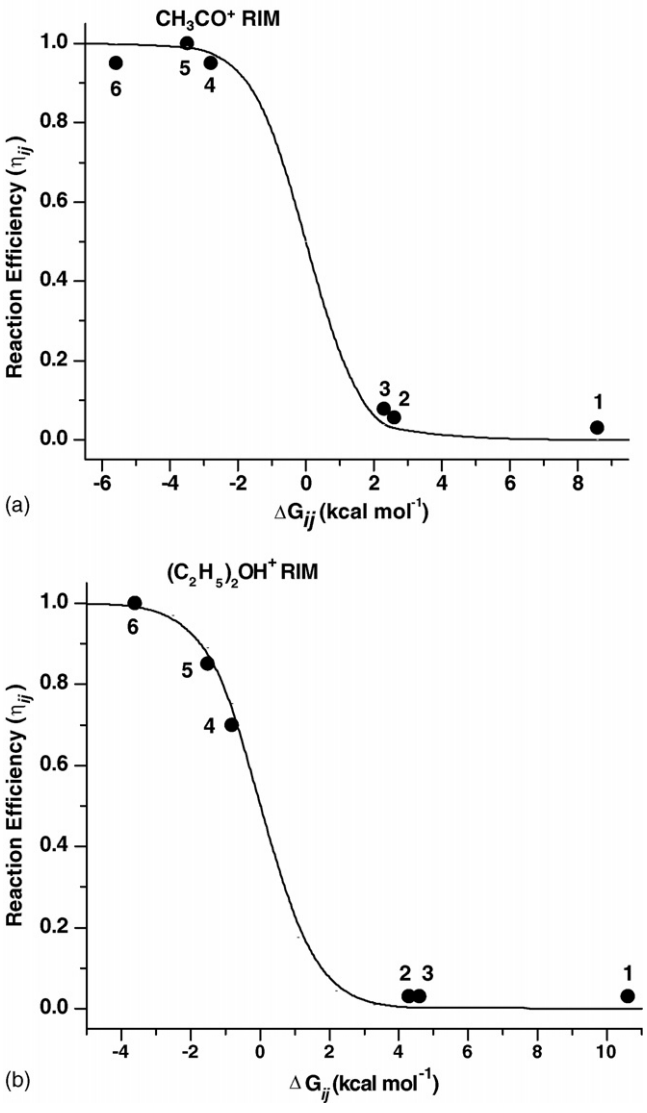

Fig. 6. Plots of MRIM determined proton transfer reaction efficiencies (η_{ij}, ●) from two reactant ions (a) CH_3CO^+ and (b) $(C_2H_5)_2OH^+$ to six analytes (1: toluene; 2: *m*-xylene; 3: acetone; 4: 3-penthanone; 5: mesitylene; 6: 4-heptanone) vs. proton transfer ergicities (ΔG_{ij}). The solid line is the theoretical proton transfer reaction efficiency calculated using Eq. (11) with $\Delta G_a = 0.0$.

erwise, the gas-phase basicity of an analyte could have been determined straightforwardly using the thermokinetic method [18]. In the alternative, plots of proton transfer reaction efficiencies (η_{ij}) from a specific reactant ion to six analytes versus the ergicities (ΔG_{ij}) are presented and discussed; the resulting plots are compared to the reaction efficiencies predicted using Eq. (11).

Plots of MRIM determined proton transfer reaction efficiencies (η_{ij}, ●) from two reactant ions CH_3CO^+ and $(C_2H_5)_2OH^+$ to six analytes versus proton transfer ergicities (ΔG_{ij}) are shown in Fig. 6a and b, respectively. In Fig. 6, labeled numbers 1 to 6 correspond to toluene, *m*-xylene, acetone, 3-penthanone, mesitylene, and 4-heptanone, respectively. The solid line is the theoretical proton transfer reaction efficiency calculated using Eq. (11) with $\Delta G_a = 0.0$. The agreement between experimental (●) and calculated (solid line) reaction efficiencies is generally excellent for our small set of reactant ions and analytes showing that $\Delta G_a = 0.0$ is a reasonable approximation for data shown in Fig. 6. A better agreement between the MRIM results and Eq. (11) is obtained if $\Delta G_a \sim -0.35$ or $0.25\,\text{kcal mol}^{-1}$ for the reactant ions CH_3CO^+ or $(C_2H_5)_2OH^+$, respectively. However, ΔG_a is small compared to other potential sources of experimental errors, e.g., the literature GB(R_i) values (e.g., see Table 1). Large experimental errors (e.g., small variations in reactant ion selected ion chromatogram amplitude not related to analyte elution) result in relatively smaller errors in determining analyte gas-phase basicities using MRIM due to the presence of natural log functions in Eqs. (9) and (10).

4.5.3. MRIM ΔG_{ij} results

A summary of MRIM calculated reaction efficiencies (η_{ij}), and ΔG_{360} results are shown in Table 2. The first two columns contain the reactant ion [R_iH^+] and analyte [A_i] and the two subsequent columns contain the MRIM calculated proton transfer reaction efficiency (η_{ij}), and ΔG_{360} values. The last two columns contain primary literature and NIST ΔG_{360} data for comparison with the present ΔG_{360} MRIM data. In our MRIM analysis, we have assigned $\eta_{ij} = 1$ for all proton transfer reactions with ergicities less than $-3.0\,\text{kcal mol}^{-1}$, i.e., to obtain reference values for ε_{Lg} used in Eq. (9).

To obtain the MRIM data on aromatic or ketone analytes shown in Table 2, multiple GC/FT-ICR experiments were performed. The variation in the MRIM determined η_{ij} values from experiment to experiment was relatively small, viz., $\Delta\eta_{ij} < 0.05\eta_{ij}$.

4.5.4. MRIM of aromatic analytes

It was observed that the reactant ion at *m*/*z* 75, protonated toluene with a reaction efficiency of ~0.03. In the present experiments, the reactant ion at *m*/*z* 75 (if protonated ether) should not be able to protonate toluene (endoergicity of $\sim 11\,\text{kcal mol}^{-1}$) at an observable rate. One can conjecture that *m*/*z* 75 may contain other protonated components (e.g., an alcohol of lower PA), or the toluene contained trace amounts of co-eluting hydrocarbons, or there is another reaction channel.

The MRIM determined $\Delta G_{360} \sim 2.0\,\text{kcal mol}^{-1}$ for the CH_3CO^+ and *m*-xylene pair was in fair agreement with

Table 2
Summary of 360 K MRIM derived proton transfer reaction efficiency (η_{ij}) and ΔG_{360} Results (comparison to literature values)

R_iH^+ (reactant ion)	A_j (analyte)	η_{ij} MRIM RE	ΔG_{ij} MRIM (kcal mol^{-1})	ΔG_{ij} primary Lit. (kcal mol^{-1})	ΔG_{ij} NIST (kcal mol^{-1})
CH_3CHOH^+	Toluene	1	<−3.0	−4.1	−5.0
	m-Xylene	1	<−3.0	−10.1	−11.0
	Acetone	1	<−3.0	−10.4	−12.2
	3-Pentanone	1	<−3.0	−15.5	−17.5
	Mesitylene	1	<−3.0	−16.5	−17.1
	4-Heptanone	1	<−3.0	−18.3	−18.8
$C_2H_5OH_2^+$	Toluene	0.95	<−2.0	ND	−3.0
	m-Xylene	1	<−2.0	ND	−9.0
	Acetone	1	<−2.0	ND	−10.2
	3-Pentanone	1	<−2.0	ND	−15.5
	Mesitylene	1	<−2.0	ND	−15.1
	4-Heptanone	1	<−2.0	ND	−16.8
CH_3CO^+	Toluene	<0.03	>2.5	8.6	8.7
	m-Xylene	0.055	2.0	2.6	2.7
	Acetone	0.077	1.8	2.3	1.5
	3-Pentanone	0.950	−2.1	−2.8	−3.8
	Mesitylene	1.000	<−2.0	−3.5	−3.4
	4-Heptanone	0.950	<−2.0	−5.6	−5.1
$(C_2H_5)_2OH^+$	Toluene	<0.03	>2.5	10.6	10.1
	m-Xylene	<0.03	>2.5	4.6	4.1
	Acetone	<0.03	>2.5	4.3	2.9
	3-Pentanone	0.700	−0.6	−0.8	−2.4
	Mesitylene	0.850	−1.2	−1.5	−2.0
	4-Heptanone	0.950	<−2.0	−3.6	−3.7

ND: no data available from primary Refs. [20–22] on GB(C_2H_5OH); MRIM: $\Delta G_{360} = RT \ln\{1/(\eta_{ij} - 1)\}$; Primary Ref.: see Table 1 for details; RE: reaction efficiency.

the primary literature ΔG_{360} value of 2.6 kcal mol^{-1} and the NIST ΔG_{360} value of 2.7 kcal mol^{-1}. The difference of ~0.6 kcal mol^{-1} between the MRIM and the primary literature or the NIST ΔG_{360} values may be the result of setting $\Delta G_a = 0.0$ (an apparent activation energy) in our analysis in Eq. (10). Using a $\Delta G_a = -0.35$ kcal mol^{-1} (see the above discussion on Fig. 6), yielded a $\Delta G_{360} \sim 2.4$ kcal mol^{-1} for the CH_3CO^+ and *m*-xylene pair which is in excellent agreement with the primary literature and NIST value of ~2.6 kcal mol^{-1}.

4.5.5. MRIM of ketone analytes

The proton transfer reaction efficiency from *m/z* 43 (CH_3CO^+) to acetone of 0.075 yielded a $\Delta G_{360} = 1.8$ kcal mol^{-1} in reasonable agreement with the primary literature ΔG_{360} value of 2.3 kcal mol^{-1} and better agreement with the NIST ΔG_{360} of 1.5 kcal mol^{-1}. The 360 K reaction efficiency of 0.075 from the present study is in excellent agreement with the 300 K reaction efficiency of 0.078 given in Ref. [31] and the averaged rate constant of 2.5×10^{-10} molecule^{-1} cm^3 s^{-1} from ref [25]. Using the $\Delta G_a = -0.35$ kcal mol^{-1} (see the above discussion on Fig. 6), yielded a ΔG_{360} for the CH_3CO^+ and acetone couple of 2.2 kcal mol^{-1} in poor agreement with the NIST value of 1.5 kcal mol^{-1}.

Using the reactant ion at *m/z* 75, the PT reaction efficiency to 3-pentanone analyte was 0.7. A reaction efficiency of 0.7 according to the thermokinetic analysis yielded a $\Delta GB = -0.6$ kcal mol^{-1}. The present $\Delta GB = -0.6$ kcal mol^{-1} is in better accord with the ΔG_{360} of ~−0.8 kcal mol^{-1} [20] compared to the NIST ΔG_{360} of ~−2.0 kcal mol^{-1} [26].

4.6. Proton affinities and gas-phase basicities by MRIM

The MRIM 360 GB(A_j) (Eq. (10)) and PA(A_j) (Eq. (13)) results were anchored using either ketene [22] or ether [20] literature basicity data. The procedure to estimate PA(A_j) by MRIM is described below in detail. Table 3 contains the PA and 360 K GB results obtained on four analytes (*m*-xylene, acetone, mesitylene and 3-pentanone) using the MRIM method and comparisons to the literature.

The proton affinity of an analyte, PA(A_j), cannot be determined in single temperature experiments (360 K in this case) without some reasonable estimation [31] of the entropy contribution (ΔS_{ij}) to $\Delta G_{ij} = \Delta H_{ij} - T\Delta S_{ij} = GB(R_i) - GB(A_j)$ (Gibbs free energy), where $\Delta H_{ij} = PA(R_i) - PA(A_j)$ and ΔS_{ij} is the equilibrium entropy change for proton exchange between R_i and A_j.

In order to calculate the MRIM PA(A_j), the entropy change, ΔS_{ij} (for the proton transfer reaction shown in Eq. (1)) is required. This can be estimated using the primary $\Delta_p S$ data in Table 1, viz., $\Delta S_{ij} = \Delta_p S^\circ(A_j) - \Delta_p S^\circ(R_i)$. Then the MRIM PA($A_j$) is given by Eq. (13), where ΔG_{ij} is the 360 K MRIM data from Table 2 (or Table 3), $\Delta G_a = 0.0$, and $T = 360$ K in our experiments:

$$PA(A_j) = PA(R_i) - \Delta G_{ij} + \Delta G_a - T\,\Delta S_{ij} \quad (13)$$

Variable temperature proton transfer equilibrium experiments have shown that $|\Delta S_{ij}|$ can be larger than 10 cal mol^{-1} K^{-1}

Table 3
Summary of 360 K MRIM derived GB and PA results and comparison to literature values

Reactant ion R_iH^+ (PA[R_i],[b] GB[R_i])[b]	Analyte, A_j	ΔG_{ij} (MRIM) (kcal mol^{-1})	ΔS_{ij} (Prim. Lit.)[a] (cal mol^{-1} K^{-1})	GB(A_j) (MRIM) (kcal mol^{-1})	GB(A_j) (Prim. Lit.)[a] (kcal mol^{-1})	GB(A_j) (NIST) (kcal mol^{-1})	PA(A_j) (MRIM) (kcal mol^{-1})	PA(A_j) (Prim. Lit.)[a] (kcal mol^{-1})	PA(A_j) (NIST) (kcal mol^{-1})
CH_3CO^+	*m*-Xylene	2.0	6.0	185.7	185.1	185.1	192.8	192.3	194.1
(197.0, 187.7)	Acetone	1.8	2.0	185.9	185.4	186.3	194.5	194.0	194.0
$(C_2H_5)_2OH^+$	3-Pentanone	−0.6	−1.0	190.3	190.5	191.6	199.1	199.3	200.0
(198.1, 189.7)	Mesitylene	−1.2	3.0	190.9	191.2	191.2	198.2	198.5	199.9

[a] $\Delta S_{ij} = \Delta_p S^\circ(A_j) - \Delta_p S^\circ(R_i)$ from the primary literature, see Table 1 for $\Delta_p S^\circ$ data and text for details.
[b] PA(R_i) or GB(R_i) in kcal mol^{-1}.

[20,32,33]; at 360 K this would contribute more than 3.6 kcal mol^{-1} to ΔG_{ij} and hence the approximation $PA(R_i) - PA(A_j) \approx \Delta G_{ij}$ is not a reasonable assumption. The absolute differences between the MRIM determined GB values for *m*-xylene, acetone, 3-pentanone, and mesitylene and the primary literature or NIST GB values lie in the range 0.2–0.6 kcal mol^{-1}. The agreement between the MRIM determined PA values and the primary literature PA values is excellent with the absolute differences laying in the range 0.2–0.5 kcal mol^{-1}. These differences may be due in part to experimental errors (both MRIM and primary literature) and setting $\Delta G_a = 0.0$ in Eqs. (10) and (13).

4.7. Estimation of amount of gas-phase analyte present in the ICR cell environs

The amount of analyte in the gas-phase (n_j) for an analyte, A_j, is given by Eq. (14):

$$n_j(\text{mol}) = [A_j]_0 V_c/(6.02 \times 10^{23}) \quad (14)$$

where $[A_j]_0$ is analyte concentration after the GC effluent pulsed valve event obtained using Eq. (6) and where V_c ($\sim$2000 cm^3) is the estimated volume of the ICR environs. To estimate the ICR cell pressure, it was reasonable to assume that the effective volume (V_c) around the ICR cell environs was about 2000 cm^3 (approximately one-third of the volume of the cell vacuum chamber). The surface area in the ICR cell environs was estimated to be $\sim$1500 cm^2 but for our purposes and to keep the kinetic model simple, analyte absorption on or desorption off surfaces in the environs of the ICR cell was not considered here.

From the analysis of the MRIM SIC data shown in Fig. 5 using Eqs. (6) and (14) (i.e., ε_{ij} values), we estimate that more than 90% of the analytes are lost to surfaces in the vicinity of the ICR cell for a $\sim$5 nmol injection on the GC. The GC peak width was approximated as a 15 s wide square wave. In other words, in our MRIM analysis, the amount of reactant depletion would have been much greater if there were no analyte losses to surfaces. The analyte losses to surfaces can be reduced by increasing the vacuum chamber temperature. The current instrumental setup and out-gassing of the heat sensitive ICR cell components, such as the transient pre-amplifier, do not allow heating the ICR cell environs beyond $\sim$90 °C.

5. Conclusions

We have demonstrated that it is possible to obtain gas-phase basicities of analytes using MRIM in GC/FT ICR MS analysis. Using a larger suite of reactant ions having smaller conjugate base gas-phase basicity increments, it should be possible to obtain analyte gas-phase basicities of near thermodynamic accuracy, ±0.5 kcal mol^{-1}. The gas-phase concentration of analytes in the FT-ICR can also be estimated using the MRIM approach. For the experiments reported here, analyte loses to surfaces were greater than 90%. In principle, MRIM could be extended to resolve co-eluting isomeric analytes using the ion-titration method [10].

Acknowledgement

This material is based upon work supported by the National Science Foundation under Grant No. CHE-0228971.

References

[1] S.D. Richardson, J. Environ. Monit. 4 (2002) 1.
[2] J. Beens, U.A.T. Brinkman, Trends Anal. Chem. 19 (2000) 260.
[3] N. Ragunathan, K.A. Krock, C. Klawun, T.A. Sasaki, C.L. Wilkins, J. Chromatogr. A 703 (1995) 335.
[4] N. Ragunathan, K.A. Krock, C. Klawun, T.A. Sasaki, C.L. Wilkins, J. Chromatogr. A 856 (1999) 349.
[5] J. Brodbelt, C.C. Liou, T. Donovan, Anal. Chem. 63 (1991) 1205.
[6] D.F. Hunt, J.F. Ryan, Chem. Commun. (1972) 620.
[7] C.W.J. Polley, B. Munson, Anal. Chem. 53 (1981) 308.
[8] V.T. Tran, B. Munson, Org. Mass Spectrom. 21 (1986) 41.
[9] A.M. Tabert, A.S. Misharin, R.G. Cooks, Analyst 129 (2004) 323.
[10] H.-H. Büker, H.-F. Grützmacher, M.E. Crestoni, A. Ricci, Int. J. Mass Spectrom. Ion Proc. 160 (1997) 167.
[11] J.E. Szulejko, T. Solouki, Anal. Chem. 74 (2002) 3434.
[12] T. Solouki, J.E. Szulejko, J.B. Bennett, L.B. Graham, J. Am. Soc. Mass Spectrom. 15 (2004) 1191.
[13] C.B. Jacoby, D.L. Rempel, M.L. Gross, Proceedings of the 38th ASMS Conference on Mass Spectrometry and Allied Topics, Tucson, AZ, USA, 1990, p. 840.
[14] J. Bennett, Undergraduate Honors Thesis, Department of Chemistry, University of Maine, Orono, ME, 2003, pp. 1–49.
[15] D.R. Lide, H.P.R. Frederikse, CRC Handbook of Chemistry and Physics, 77th ed., CRC Press Inc., Baton Rouge, LA, 1996–1997, Section 10-210, ISBN 0-8493-0477-6.
[16] F. Hatch, B. Munson, J. Phys. Chem. 82 (1978) 2362.
[17] Y. Lin, G.R. Nichol, D.P. Ridge, Eur. J. Mass Spectrom. 1 (1995) 113.
[18] G. Bouchoux, J.Y. Salpin, D. Leblanc, Int. J. Mass Spectrom. Ion Proc. 153 (1996) 37.
[19] G.S. Gorman, I.J. Amster, Org. Mass Spectrom. 28 (1993) 1602.
[20] J.E. Szulejko, T.B. McMahon, J. Am. Chem. Soc. 115 (1993) 7839.
[21] J.E. Szulejko, J. Hrušák, T.B. McMahon, J. Mass Spectrom. 32 (1997) 494.
[22] A.L.L. East, B.J. Smith, L. Radom, J. Am. Chem. Soc. 119 (1997) 9014.
[23] P.C. Burgers, J.L. Holmes, J.E. Szulejko, A.A. Mommers, J.K. Terlouw, Org. Mass Spectrom. 18 (1983) 254.
[24] M.N. Danchevskaya, S.N. Torbin, Adv. Mass Spectrom. 7B (1978) 1314.
[25] V. Anicich, Jet Propulsion Laboratory Databases, 2003 (CD).
[26] Chemistry Online Webbook, 2005. http://nist.gov.
[27] D.K. Bohme, Int. J. Mass Spectrom. Ion Proc. 115 (1992) 95.
[28] J.H. Moore, C.C. Davis, M.A. Coplan, Building Scientific Apparatus: A Practical Guide to Design and Construction, 2nd ed., Addison-Wesley, New York, 1995, p. 78.
[29] J.E. Bartmess, R.M. Georgiadis, Vacuum 33 (1983) 149.
[30] M.S. Ahmed, R.C. Dunbar, J. Chem. Phys. 89 (1988) 4829.
[31] G. Bouchoux, J.-Y. Salpin, J. Phys. Chem. 100 (1996) 16555.
[32] J.E. Szulejko, T.B. McMahon, V. Troude, G. Bouchoux, H.E. Audier, J. Phys. Chem. A 102 (1998) 1879.
[33] G. Bouchoux, J.-F. Gal, P.C. Maria, J.E. Szulejko, T.B. McMahon, J. Tortajada, A. Luna, M. Yanez, O. Mo, J. Phys. Chem. A 102 (1998) 9183.